Design and Analysis of a Low-Loss Linear Analog Phase Modulator for Deep Space Spacecraft X-Band Transponder Applications

N. R. Mysoor and R. O. Mueller
Spacecraft Telecommunications Equipment Section

This article summarizes the design concepts, analyses, and development of an X-band (8145 MHz) transponder low-loss linear phase modulator for deep space spacecraft applications. A single-section breadboard circulator-coupled reflection phase modulator has been analyzed, fabricated, and evaluated. A linear phase deviation of 92 deg with a linearity tolerance of ±8 percent was measured for this modulator from 8257 MHz to 8634 MHz over the temperature range −20 deg C to +75 deg C. The measured insertion loss and the static delay variation with temperature were 2 ±0.3 dB and 0.16 psec/deg C, respectively. Based on this design, cascaded sections have been modeled, and simulations were performed to provide an X-band deep space transponder (DST) phase modulator with ±2.5 radians (±143 deg) of peak phase deviation to accommodate downlink signal modulation with composite telemetry data and ranging, with a deviation linearity tolerance of ±8 percent and insertion loss of less than 10 ±0.5 dB. A two-section phase modulator using constant gamma hyperabrupt varactors and an efficient modulator driver circuit was breadboarded. The measured results satisfy the DST phase-modulator requirements and show excellent agreement with the predicted results.

I. Introduction

A circulator-coupled reflection phase modulator has been analyzed and investigated to provide the capability to directly modulate an X-band (8415 MHz) downlink carrier for the next generation of spaceborne communications systems. The phase modulator must be capable of large linear phase deviation, low loss, and wideband operation with good thermal stability. In addition, the phase modulator and its driver circuit must be compact and consume low dc power. The design is to provide ±2.5 radians (±143 degrees) of peak phase deviation to accommodate downlink modulation of telemetry and ranging signals. The tolerance on the phase deviation linearity is ±8 percent. The insertion loss should be less than 10 dB, and its variation with phase shift should be

within ±0.5 dB. The phase delay variation specifications over the transponder hardware qualification environment, −20 deg C to +75 deg C, are less than 32 psec/deg C for the transponder, and less than 0.5 psec/deg C for the phase modulator. Such stringent specifications make the hardware implementation rather difficult. This investigation, which updates research described in [1], considers the reflection-type phase shifter for the implementation of the hardware. The results extrapolated from analyses and measured performance for a single-section phase modulator with high phase-resolution capability are presented in this article. Theoretical analyses of the modulator are presented in Section II, the breadboard modulator configuration and test data are presented in Section III, and the conclusions are presented in Section IV.

II. Phase Modulator Analyses

This investigation considers the circulator-reflection-type phase shifter. A single-stage phase shifter is shown in Fig. 1. Theoretical analyses of the single-stage and multistage phase-modulator circuits are presented in the following subsections. Both abrupt-junction and hyperabrupt-junction varactors will be considered.

A. Analysis of a Single-Stage, Reflection Phase Modulator

The varactor diode is well suited for the phase modulator [2,3] application because it can provide rapid phase change with the applied voltage. The circuit model for a packaged diode terminating a transmission line of characteristic impedance, Z_o, for a reflective phase shifter is shown in Fig. 2. The junction capacitance of varactor tuning diodes is modeled as

$$\frac{C_j(V)}{C_o} = \left(1 + \frac{|V|}{\Phi}\right) - \Gamma$$

where $C_j(V)$ is the junction capacitance at reverse bias voltage, V. The absolute value of the applied reverse bias voltage is $|V|$. Additionally, C_o is the junction capacitance at $V = 0$, and Φ is the built-in potential, which is equal to 0.8 V for silicon and 1.3 V for gallium arsenide. The diode capacity variation parameter, Γ, is the slope of the capacitance-voltage ($C - V$) curve when plotted on log–log scaled paper. This slope (Γ) is a function of the bias voltage and junction temperature. In the operating bias range of the diode, Γ can be treated as a constant.

1. Silicon Abrupt Junction Varactors. The diode capacity parameter Γ is equal to about 0.5 for practical abrupt-junction silicon diodes. For this analysis, an abrupt-junction silicon diode of capacitance C_j equal to 0.6 pF at −4 V bias is considered. Shown in the circuit model [1] of Fig. 2 are the diode junction capacitance, diode leakage resistance (R_s), package inductance (L_p), package capacitance (C_p), lead inductance (L_l), parallel resistance (R_p), and 10-ohm transmission line. To obtain a large linear phase shift, it is necessary to use a low-impedance transmission line at the diode terminal. The 10-ohm line was selected because it can be realized on a 0.254-mm-thick alumina substrate. Furthermore, its line width is not overly wide as compared with line length and the diameter of the device package. The line impedances and lengths are optimized to provide linear phase-shift variation with bias voltage. The low parasitic packages used in this investigation are Alpha Associates 304-001 and Microwave Associates MA-96 packages. The typical values of package parasitics for these packages are: L_p = 0.15 nH and C_p = 0.17 pF. The contact lead inductance L_l = 0.05 nH. The device series resistance R_s is a function of Q. The following expression for Q as a function of the bias voltage, V, was obtained by curve fitting the manufacturer's (Alpha Associates') data at 50 MHz:

$$Q(V) = 1700 + 875|V|$$

The diode series resistance is then given by:

$$R_s(V) = [2\pi \times (50 \times 10^6) Q C_j(V)]^{-1}$$

The parallel resistance R_p at the diode plane is intentionally added to maintain the insertion loss constant. The calculated phase shift and insertion loss variations with the bias voltage for this model are shown in Fig. 3. The phase shift is linear over the 4.5 ±2.5 V bias range. The linear phase shift over this range is ±50 degrees. The maximum deviation from linearity is within ±8 percent. The insertion loss variation over this voltage range is 1.8 ±0.15 dB. This insertion loss does not include the losses due to the circulator and transmission line matching sections. The insertion loss of a phase modulator must be kept constant with phase shift. The variation of the insertion loss with phase shift causes amplitude modulation (AM) of the RF signal. This AM may be converted to undesirable phase modulation (PM) by subsequent nonlinear operation.

2. Gallium Arsenide Constant Gamma Hyperabrupt Varactors. The gamma of typical hyperabrupt varactors varies widely with applied voltage, which makes

these varactors unsuitable for linear phase-modulator applications. Recent processing developments have enabled the construction of varactors with gammas that remain constant over a limited voltage range. The varactors of constant Γ equal to 1.25 and 1.5 have been analyzed. Both were simulated by using the following package (MA-96) parasitics: $C_{-4V} = 0.6$ pF, $C_p = 0.17$ pF, and $L_p = 0.15$ nH. The expression for Q that was used in the simulation was obtained by curve fitting the manufacturer's (Microwave Associates') data at 50 MHz.

$$Q(V) = 1538 - 115.6|V| + 118.2|V|^2 + 21.96|V|^3 - 1.683|V|^4$$

The optimum characteristic impedance of the transmission line connected to the varactor is 30 ohms; this value provides flat insertion loss and large linear phase shift over the designed bias range. The simulation results for single-section hyperabrupt varactors are shown in Fig. 3. Linear operation is obtained at 4.5 ±2.5 V, which results in a phase shift of ±75 deg (< 8 percent linearity deviation) and an insertion loss of 1.3 ±0.05 dB for a gamma of 1.5. The results also show that a gamma of 1.5 yields a loss that is 0.2 dB lower than a gamma of 1.25, although both have the same linearity and AM characteristics. The higher gamma value provides a more linear tuning characteristic, which results in a more sensitive phase modulator: 30 deg/V as compared with 20 deg/V for a gamma of 0.47.

B. Analysis of Multistage Reflection Phase Modulator

Comparisons of ±143-deg multisection phase shifters for various diode gamma values are given in Fig. 4 and Table 1. The results do not include the losses due to circulators and isolators and show that only two sections utilizing constant gamma hyperabrupt varactors have to be cascaded, as compared with three sections for the abrupt junction case. The predicted phase sensitivity for these cases is equal to 60 deg/V. The lowest insertion loss of 2.55 ±0.1 dB is predicted for the two-section varactor modulator with a constant gamma of 1.5.

III. Phase Modulator Implementation and Performance

The circuit configuration and measured performances of the breadboard single-stage and two-section circulator reflection phase modulators are given in subsections III.A and III.B. The performance of the modulator driver circuit is presented in subsection III.C.

A. Single-Stage Circulator Reflection Phase Modulator

1. Circuit Configuration. The circuit diagram and a photograph of the phase modulator (with abrupt junction varactors) are shown in Figs. 1 and 5, respectively. The reflection phase shifter configuration [2,3] makes use of a 50-ohm circulator to provide matched input and output terminals for the phase-shifting diode circuit in the middle path. The circulator used in this investigation is a broadband 8.4 to 12 GHz circulator (Western Microwave, Inc., 13CX-481, Serial no. 10). The two-way insertion loss of the circulator is 0.6 ±0.1 dB over the operating bandwidth at the nominal temperature of 23 deg C. The circuit (Fig. 1) consists of a packaged diode at the end of a 10-ohm line and two quarter-wave matching sections (33.44-ohm and 14.95-ohm sections) to transform 10 ohms at the diode terminals to 50 ohms at the circulator port. The 10-ohm microstrip circuit is etched on a 0.254-mm-thick-Roger 6010.5 substrate of dielectric constant $K = 10.5$. The width of the 10.0-ohm line is 2.464 mm, which is slightly (20 percent) larger than the diode package diameter of 2.03 mm. Better than 75 percent size matching between the diode and the line width is necessary in hybrid circuits to reduce insertion loss. The diode's anode is soldered to the ground as shown in Fig. 5. The circuit model for the diode, diode package parasitics, and connecting lead inductance are illustrated in Fig. 2. The junction capacitance of the selected abrupt-junction silicon diode (Alpha Industries, DVH 6733-02 in 168-001 package) is approximately equal to 0.6 pF at −4 V bias, 0.45 pF at −8 V bias, and 1.392 pF at 0 V bias. This results in a diode capacitance ratio of 3:1 from 0 V to −8 V bias range. Such large capacitance variation with bias is necessary to obtain large phase deviation. The series resistance of the diode is 3.6 ohms. The phase deviation characteristics of the circuit are also influenced by the values of package parasitics, interconnection lead inductance, and the length of the 10.0-ohm line. The typical values of the diode package parasitics supplied by the manufacturer are: $Lp = 0.5$ nH and $Cp = 0.18$ pF. The inductance of the interconnection lead (L_l) between the diode package and the 10.0-ohm line is equal to 0.05 nH. It is difficult to accurately model the package parasitics. The lengths of the interconnection lead (L_l) and the 10.0-ohm line can be adjusted to obtain linear phase deviation.

2. Performance of Single-Stage Phase Modulator at 8415 MHz. The measured phase deviation versus bias characteristics for the single-section phase modulator (Fig. 5) with an abrupt junction varactor is illustrated in Fig. 6. The nominal values of frequency, bias, voltage, and temperature in these measurements are 8415 MHz, +4.5 V and +23 deg C, respectively. The measurement band-

width ranged from 8257 MHz to 8634 MHz. The phase angle measured at 0 V bias, and the nominal frequency 8415 MHz was used as the reference angle. The measured linear phase deviation for the voltage swing ±3 V above the nominal bias of 4.5 V was ±46 deg with a linearity better than ±8 percent of a best-fitted straight line. The phase-modulator circuit was subjected to temperature tests over the hardware qualification temperature range from −20 deg C to +75 deg C. As shown in Fig. 7, the overall variation of the static phase with temperature is about 45 deg with 0.5 deg/deg C slope. The calculated static phase delay at 8415 MHz is 0.16 psec/deg C. As seen from Fig. 7, the change in the static phase with temperature is not symmetrical about its value at +23 deg C. The reason is that the static phase variation of the circulator with temperature is nonlinear. The measured value of the circulator's static phase shift was 2.2 deg for a change in temperature from +23 deg C to +75 deg C, and was equal to −17.3 deg from +23 deg C to −20 deg C. But the temperature-induced phase shift for the diode circuit has a linear slope equal to 0.26 deg/deg C. Measured insertion loss as a function of varactor bias and temperature is shown in Fig. 7. The RF input power level was equal to 5 dBm at 8415 MHz. The maximum variation of the insertion loss with the circulator was found to be 2 ±0.3 dB over the bias levels (4.5 ±3 V), temperature range (−20 deg C to +75 deg C), and the RF range (8257 MHz to 8634 MHz). This includes the circulator's two-way insertion loss of 0.6 dB. The diode phase shift and linearity can be calculated if all the circuit component values are known fairly accurately. The values of package parasitics and the diode's junction dynamics are not well known, which results in a discrepancy between the measured and predicted results.

B. Two-Stage Circulator Reflection Phase Modulator

A two-stage phase modulator with a 1.5-gamma hyperabrupt varactor was breadboarded and tested at X-band. The two-stage phase modulator schematic and assembly are illustrated in Figs. 8 and 9, respectively. The circuit layout is etched on a 0.508-mm-thick RT/Duroid 6002 soft substrate of dielectric constant $K = 2.94$. The constant 1.5 gamma varactor (Microwave Associates MA 46471-96) is mounted with a contact strip at the end of an optimized 30-ohm, 2.79-mm-wide transformer. The diode capacitance at −4 V is equal to 0.65 pF. TRACK 6.35-mm flange micropuck circulators (79*9001) and isolators (89*9001) are used in this breadboard. Their measured port-to-port one-way insertion loss is 1 ±0.1 dB. The measured values of phase deviation and insertion loss for the phase modulator are compared with the predicted results in Fig. 10. The measurements were conducted by using a test RF signal level of +9 dBm. The insertion loss for this unit is 8.3 ±0.5 dB, the phase deviation is ±150 deg, with a linearity better than ±8 percent for a bias voltage range of 4.5 ±2.5 V. The model accurately predicted a linear phase slope of 60 deg/V. The predicted insertion loss, including circulator and isolator losses, is 7.4 ±0.4 dB, which is about 0.9 dB lower than the measured values. The discrepancy in the insertion loss probably resulted from the unaccounted-for interconnecting microstrip and radiation losses. The measured phase-delay variation is 0.252 psec/deg C over the design temperature range of −30 deg C to +85 deg C. The size of the breadboard modulator is 61×36×14.3 mm (Fig. 9). The driver circuit is not included in this breadboard layout.

C. Phase-Modulator Op-Amp Driver Circuit

The phase-modulator driver circuit schematic is shown in Fig. 11. The functions of the phase-modulator drive circuit are to sum and amplify the modulation input signals and to provide composite drive voltage to the varactor diodes. The modulation input signals include the spacecraft telemetry, ranging, and differential one-way ranging (DOR) signals. The modulation frequency ranges from 1 kHz to 20 MHz. The selected wideband op-amp for this application is Comlinear CLC 505. The size of the modulator driver circuit is 38×25×14.3 mm.

Figure 12 shows the predicted and measured gain versus frequency characteristics of the phase-modulator driver circuit at −35 deg C, +25 deg C, and +85 deg C. The measured response is flat and drops only 0.4 dB, from 0.5 MHz to 20 MHz. The measured 3-dB bandwidths at −35 deg C, +25 deg C, and +85 deg C are 92 MHz, 84 MHz, and 75 MHz, respectively. The measured results are actually better than the circuit response predicted by the Simulation Program with Integrated Circuit Emphasis (SPICE) model. The model correctly predicted higher gain at lower temperatures. The dc power consumption with an 8-volt peak-to-peak output swing is 112 mW; when no signal is applied, the power consumption is 32 mW.

IV. Conclusions

Single-section and two-section analog X-band reflection phase modulators were developed. The phase modulator performance is accurately predicted by the theoretical modeling and simulations. By using a given package-type abrupt-junction varactor diode and a circulator, a phase modulator was realized. From 8257 MHz to 8634 MHz, the measured voltage-controlled linear phase deviation, linearity tolerance, and insertion loss were ±46 deg, ±8 percent,

and 2 ±0.3 dB, respectively, over the test temperature range of −20 deg C to +75 deg C. The static phase delay was found to be 0.16 psec/deg C. By using hyperabrupt junction varactor diodes of a constant gamma of 1.5, a full ±2.5 radian deviation phase modulator was realized by cascading two phase-shifter circuits. From 8400 to 8500 MHz, the measured phase shift and insertion loss are ±2.5 radians with better than ±8 percent linearity and 8.3 ±0.5 dB, respectively. An efficient phase modulator driver circuit was also developed and tested. The measured gain-frequency characteristics over the design temperature range agreed well with the predicted results. The modulator driver 3-dB bandwidth and dc power consumption at 25 deg C are 84 MHz and 112 mW, respectively.

Acknowledgments

The authors gratefully acknowledge the valuable support and comments of A. W. Kermode during the course of this work. The authors also thank Mark Bockmann of Motorola (Strategic Electronics Division, Chandler, Arizona) for the phase-modulator breadboard implementation.

References

[1] N. R. Mysoor, "A Low-Loss Linear Analog Phase Modulator for 8415 MHz Transponder Applications," *TDA Progress Report 42-96,* vol. October–December 1988, Jet Propulsion Laboratory, Pasadena, California, pp. 172–178, February 15, 1989.

[2] R. Garver, "360° Varactor Linear Phase Modulator," *IEEE Trans. Microwave Theory Tech.,* vol. MTT-17, pp. 137–147, March 1969.

[3] R. Garver, "Broad-Band Diode Phase Shifters," *IEEE Trans. Microwave Theory Tech.,* vol. MTT-20, pp. 314–323, May 1972.

Table 1. Summary of predicted performance for multiple section phase modulators

Varactor gamma	Phase shift, deg	Linearity, percent	Insertion loss, dB	Insertion loss variation, dB	Sensitivity, deg/V	Nominal bias voltage, Vdc	Modulation swing, V	Number of sections
0.47	±140	< ±8	5.35	±0.15	60	4.5	±2.5	3
1.25	±143	< ±8	2.9	±0.08	60	4.5	±2.5	2
1.5	±142	< ±8	2.55	±0.1	60	4.5	±2.5	2
Specification	±143.5	< ±8	10 dB max	±0.45	57	—	—	

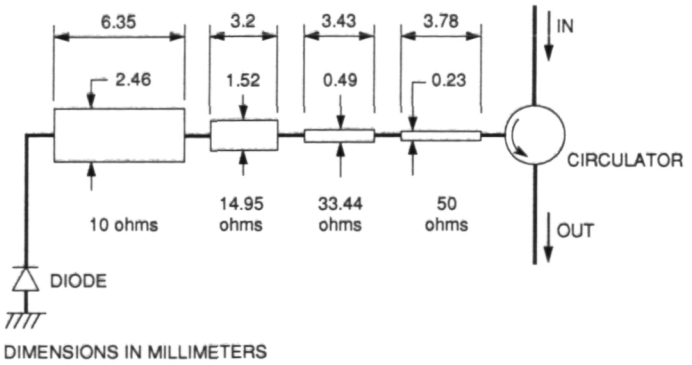

Fig. 1. Phase modulator circuit layout etched on a 0.254-mm-thick soft substrate dielectric constant K = 10.5.

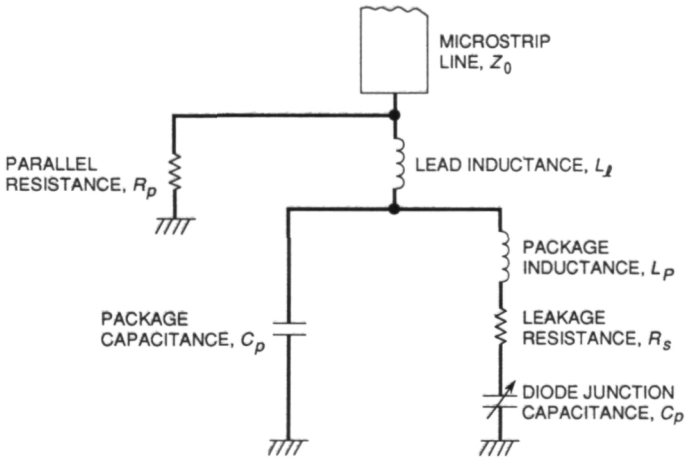

Fig. 2. Phase modulator circuit model.

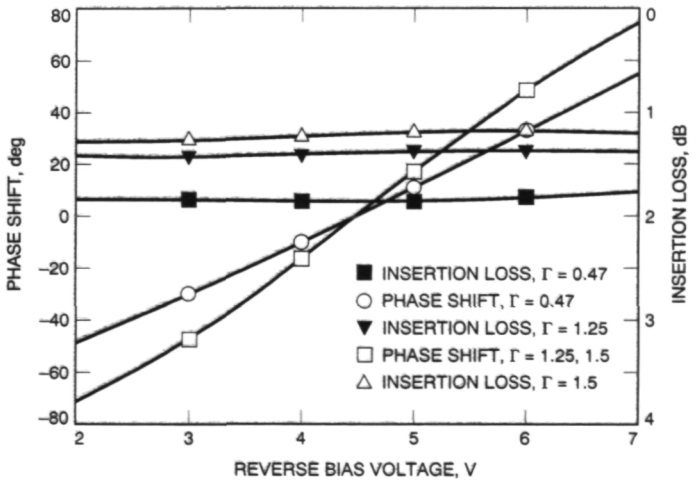

Fig. 3. Predicted phase shift and insertion loss as a function of reverse bias voltage for a single-section phase modulator for three different values of gamma.

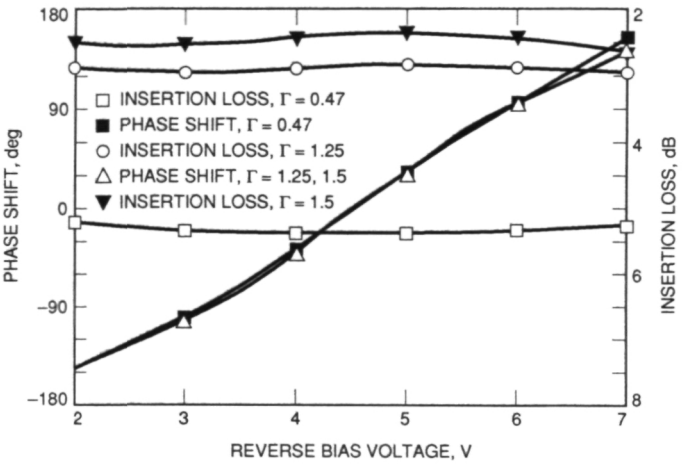

Fig. 4. Predicted phase shift and insertion loss for a two-section phase modulator with $\Gamma = 1.25, 1.5$, and for a three-section phase modulator with $\Gamma = 0.47$.

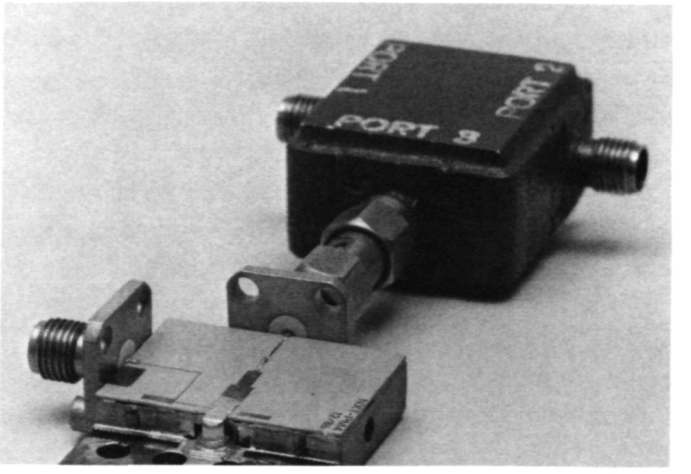

Fig. 5. X-band (8415 MHz) phase modulator.

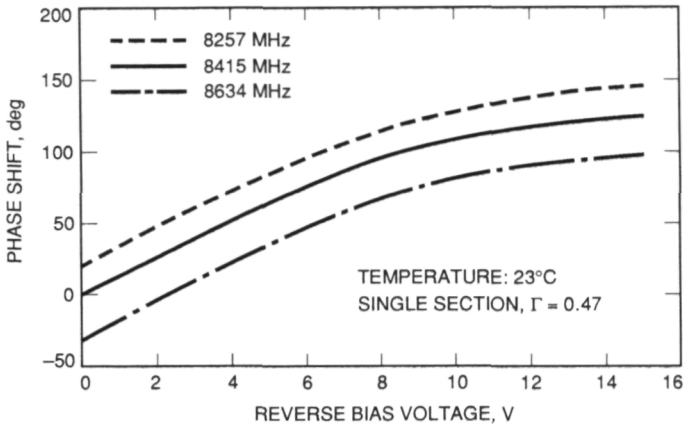

Fig. 6. Measured phase shift as a function of dc bias voltage and frequency.

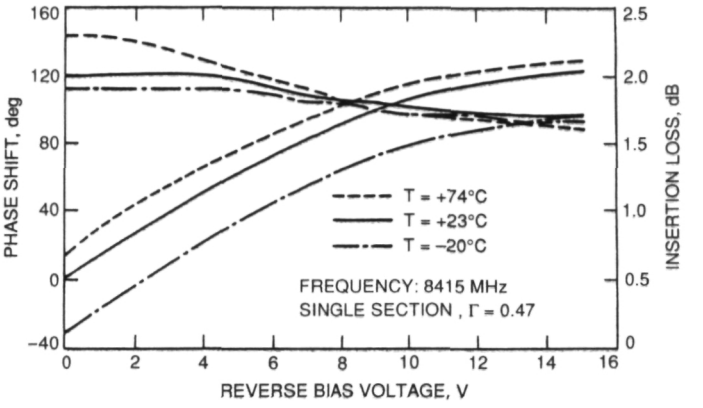

Fig. 7. Measured phase shift versus dc bias voltage and temperature.

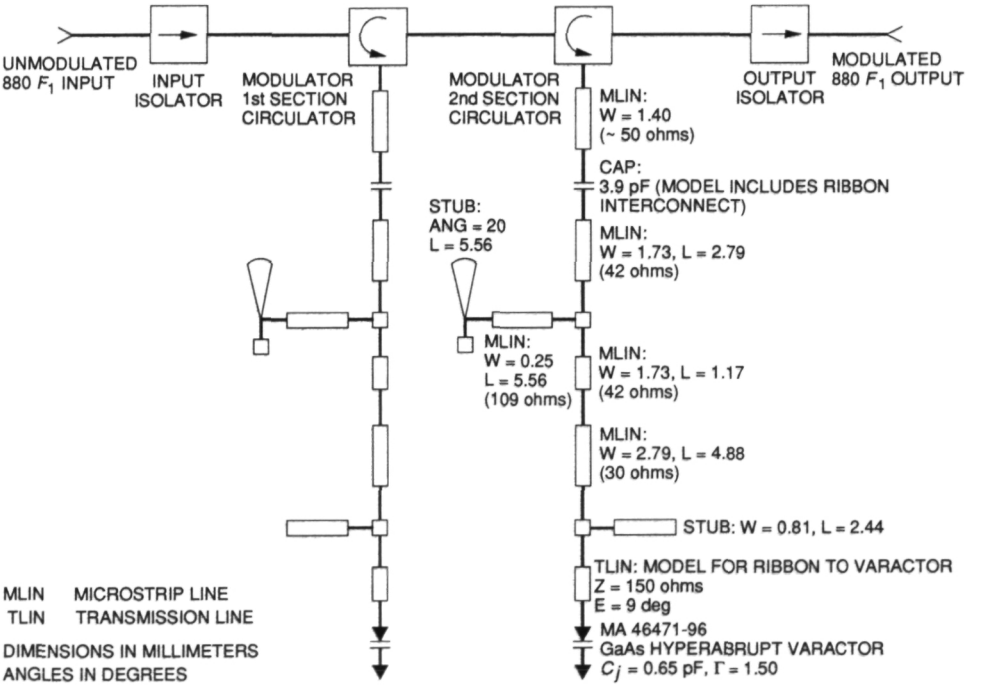

Fig. 8. Deep Space Spacecraft Transponder X-band (8415-MHz) phase modulator schematic.

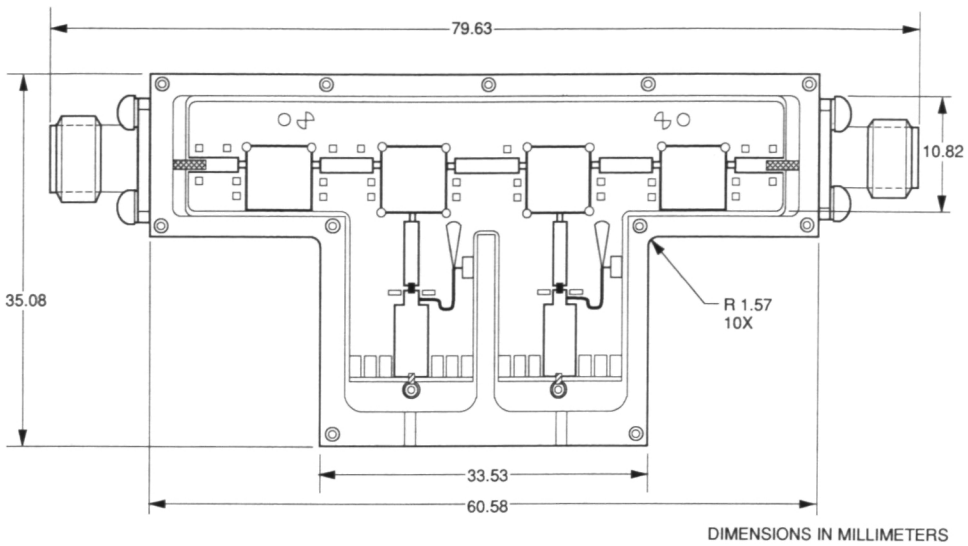

Fig. 9. Deep Space Spacecraft Transponder phase modulator assembly.

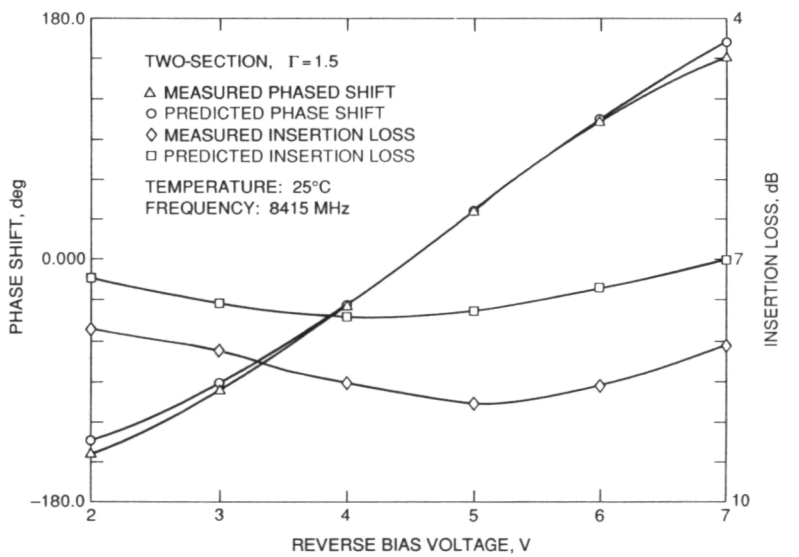

Fig. 10. Measured and predicted results for the two-section phase modulator.

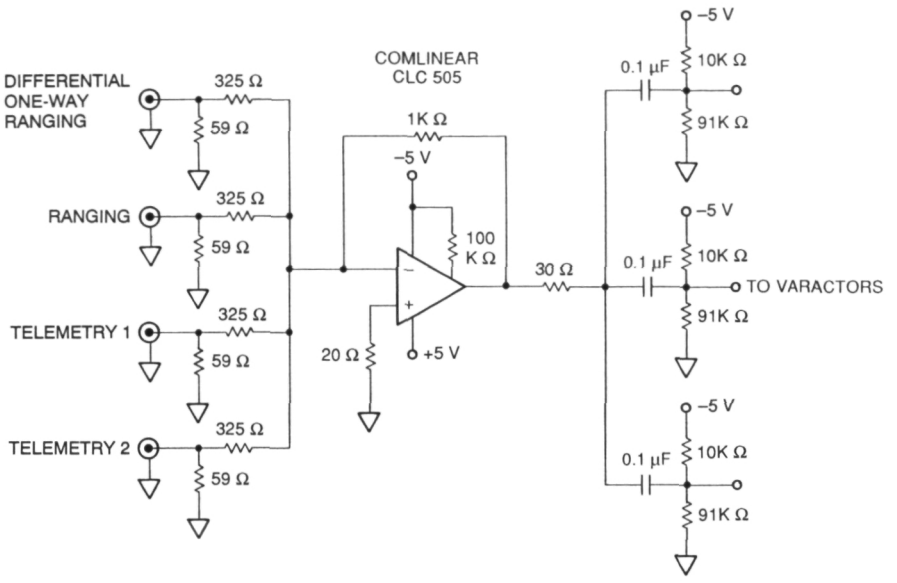

Fig. 11. Deep Space Spacecraft Transponder phase modulator driver circuit schematic.

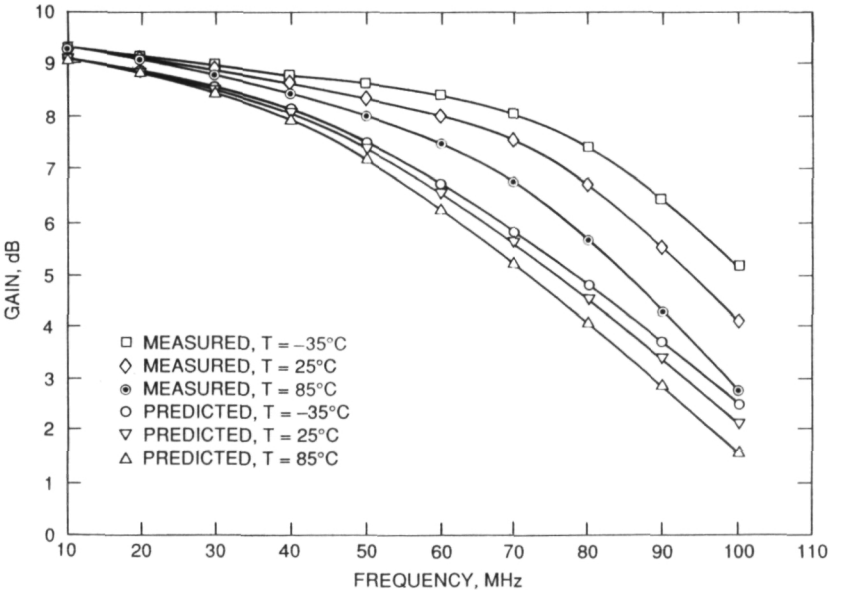

Fig. 12. Measured and predicted gain versus frequency for the phase modulator driver circuit.